State to state He–CO rotationally inelastic scattering

Stiliana Antonova,[a] Ao Lin, Antonis P. Tsakotellis, and George C. McBane
Department of Chemistry, The Ohio State University, Columbus, Ohio 43210

(Received 15 September 1998; accepted 27 October 1998)

Relative integral cross sections for rotational excitation of CO in collisions with He were measured at energies of 72 and 89 meV. The cross sections are sensitive to anisotropy in the repulsive wall of the He–CO interaction. The experiments were done in crossed molecular beams with resonance enhanced multiphoton ionization detection. The observed cross sections display interference structure at low Δj, despite the average over the initial CO rotational distribution. At higher Δj, the cross sections decrease smoothly. The results are compared with cross sections calculated from two high quality potential energy surfaces for the He–CO interaction. The *ab initio* SAPT surface of Heijmen *et al.* [J. Chem. Phys. **107**, 9921 (1997)] agrees with the data better than the XC(fit) surface of Le Roy *et al.* [Farad. Disc. **97**, 81 (1994)]. © *1999 American Institute of Physics.* [S0021-9606(99)00105-1]

I. INTRODUCTION

This article presents experiments that are sensitive to anisotropy in the repulsive part of the He–CO interaction. Thachuk *et al.* gave a thorough review of experimental and theoretical work on He–CO interactions in their 1996 paper.[1] We will give a brief review that concentrates on developments since then and on the work most relevant to the repulsive part of the potential energy surface.

The first molecular beam experiment on He–CO collisions was the 1971 total scattering cross section measurement of Pauly *et al.* over the energy range 1–100 meV, which detected no effects of anisotropy.[2] Pressure broadening data reported by Nerf and Sonnenberg in 1975 were the first experimental data sensitive to the anisotropy of the He–CO potential.[3] In 1979 Keil *et al.* measured total differential cross sections for He–CO scattering and estimated a single anisotropy parameter.[4] In 1980 Faubel *et al.* published a time-of-flight spectrum of He scattered from CO at one laboratory angle that showed partial resolution of the CO rotationally inelastic transitions.[5] Transitions up to $\Delta j = 3$ were apparent at their collision energy of 27.3 meV. Around the same time Bassi *et al.* studied rotational relaxation of CO in a free jet of He with infrared spectroscopy.[6]

Thomas *et al.* published an *ab initio* potential energy surface (''TKD'') in 1980 that served as the standard for about fifteen years.[7] With minor modifications suggested by Dilling[8] and Gianturco *et al.*,[9] it matched the available scattering, pressure broadening, and bulk property data satisfactorily.

In 1994, McKellar and co-workers reported a high resolution infrared spectrum of the He–CO van der Waals complex.[10] The TKD potential was unable to explain the observed spectrum, so McKellar *et al.* developed a new empirical surface, called $V_{(3,3,3)}$, by fitting an analytic model to the spectrum. Le Roy *et al.* then fitted a different potential model, the exchange-Coulomb (XC) model, to the same spectrum and obtained equally good agreement with the spectroscopic observations.[11] The XC model uses a physically sensible form in the repulsive region and so might provide a good representation there even though the IR data to which it was fitted are not sensitive to that region.

Three new *ab initio* potentials appeared between 1994 and 1996.[12–14] Thachuk *et al.*[1] and Dham and Meath[15] subsequently tested the different potentials' predictions against several experimental observables and found that the XC(fit) potential was at least as good as the others.

Since the comparative study of Thachuk *et al.*, two new sets of experimental measurements have appeared: thermal diffusion constants measured by Gianturco *et al.*,[16] and a much more complete IR spectrum from Chan and McKellar.[17]

Heck and Dickinson[18] and Gianturco *et al.*[16] tested several potential surfaces against a variety of transport property measurements, concentrating on data that should be sensitive to the repulsive wall of the potential. They agree that the XC(fit) potential works as well as any, and that the modified TKD potential that Gianturco *et al.* call POT11 has deficiencies in the attractive well.

In addition, Heijmen *et al.* developed a new *ab initio* potential[19] by symmetry adapted perturbation theory (SAPT); it is an improved version of the earlier SAPT surface of Moszynski *et al.*[12] that was used in several of the comparative studies. This new surface includes the dependence on the CO vibrational coordinate (as most others do not) and is probably the most accurate *ab initio* one now available. The grid of nuclear arrangements used in the quantum chemistry calculations extended into the repulsive region to a minimum distance of 5 bohr. The SAPT potential predicts the He–CO infrared spectrum with a maximum line position error of 0.1 cm^{-1} and an rms deviation of 0.038 cm^{-1}, so its accuracy in the well region is nearly as good as that of the XC(fit) potential. Reid *et al.* used this new surface to evaluate temperature-dependent vibrational deactivation rate coefficients and found that it described the qualitative

[a]Present address: Department of Physics, Bryn Mawr College, Bryn Mawr, PA 19010.

behavior well though it was not in complete agreement with the experiments.[20] Their results support optimism that the repulsive part of the potential may be accurately represented by the SAPT surface.

Very recently Gianturco *et al.* calculated a new He–CO surface by a mixture of relatively inexpensive *ab initio* methods.[21] Their potential agrees fairly closely with the preliminary SAPT potential of Moszynski *et al.* in the repulsive region, but disagrees in the van der Waals well. It has not been tested against the infrared spectra.

In this article we report measurements of state to state integral cross sections for rotationally inelastic He–CO collisions at 72 and 89 meV. These cross sections are sensitive to the shape of the repulsive wall, and have the advantage that they can be computed with confidence from any potential surface. We compare our experimental results with predictions of the two best available potential surfaces, the XC(fit) potential of Le Roy *et al.* and the new SAPT potential of Heijmen *et al.*. The previous measurements most closely related to ours are the rotationally inelastic TOF spectra of Faubel *et al.*[5] and the relative total $T \rightarrow R$ cross sections measured in crossed supersonic jets by Kruus.[22]

Oscillatory structure in the postcollision rotational distributions is prominent in our results. Brumer identified oscillations in calculated H+HCN cross sections as interference effects related to near-symmetry of the potential surface in 1974.[23] Green and Thaddeus saw similar oscillations in their computational study of low energy He–CO collisions,[24] and Augustin and Miller pointed out that the oscillations must be due to interference since they did not appear in classical trajectory calculations.[25] McCurdy and Miller then used classical *S*-matrix theory to show[26] that the structure appears because of interference between collisions at the two ends of the CO molecule. In the homonuclear limit, the interference is complete and results in the well known restriction to even Δj. In heteronuclear molecules, either even or odd Δj can be favored, and the propensity can change from one to the other as Δj changes. The propensities are determined by competition between terms with even and odd orders in the Legendre expansion of the potential. Maricq[27] and Alexander and co-workers[28,29] have also discussed the effect.

Andresen *et al.* observed this interference first in experiments on Ar–NO(X) collisions.[30,31] Similar structure also appears in later data on NO(X),[32,33] NO(A),[32] CN(X),[34] and CN(A)[35–37] collisions. The interference oscillations do not change rapidly as the collision energy changes, so they are fairly robust toward experimental averages over collision energy. They can, however, be washed out easily by imperfect exerimental preparation of a single precollision state. Double resonance collision experiments provide nearly ideal initial state preparation, but with a wide range of collision energies. Crossed molecular beam experiments, on the other hand, define the collision energy well but their success at clean initial state preparation varies. Macdonald and Liu[38] therefore interpreted the absence of oscillations in their NCO–He crossed beam data cautiously. The double resonance results of Smith and Johnson[32] on NO(A)–He showed no oscillations though oscillations were present for the other rare gas colliders; the lack of alternations in the He data certainly reflects properties of the NO(A)–He potential surface. In the crossed beam work presented here, the amplitudes of the interference oscillations remaining after the average over the precollision state distribution serve as sensitive probes of the He–CO potential surface.

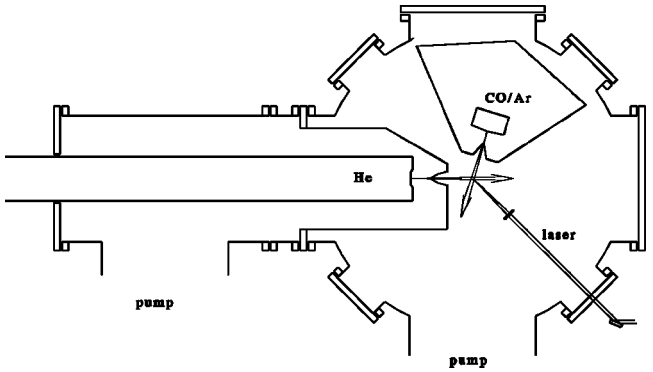

FIG. 1. Schematic diagram of the apparatus. The source chamber for the CO/Ar valve is evacuated by a pump behind the plane of the figure. The ion flight path extends out of the plane.

II. EXPERIMENT

Two skimmed supersonic beams, one of pure He and the other of CO diluted in argon, intersected in a high vacuum chamber. The changes in the rotational populations of CO caused by collisions were determined by resonance enhanced multiphoton ionization (REMPI). Figure 1 shows a simple diagram of the apparatus.

A 5%CO/95%Ar mixture expanded from a piezoelectric valve of the Proch and Trickl design.[39] The valve was mounted rigidly in a chamber attached to a large rotatable disk, and the beam traveled parallel to the surface of the disk. Different orientations of the disk provided different intersection angles between the CO and He beams. Intersection angles of 107° and 140° provided center of mass collision energies of 72 and 89 meV (583 and 720 cm^{-1}), with $\Delta E/E$ of about 6%. The valve nozzle was 25 mm from a conical skimmer with a 1.5 mm diameter orifice (Beam Dynamics) and was 79 mm from the center of the scattering chamber. The pressure of the CO/Ar mixture was 3.7 bar throughout the experiments. The pulse width as measured by a fast ionization gauge (Beam Dynamics) was about 100 μs, though the coldest part of the beam as measured by REMPI on the $S(0)$ transition had a FWHM of only 55 μs.

The He beam was produced by a commercial pulsed valve of the current-loop design (R. M. Jordan). It was skimmed by a homemade rectangular skimmer with a 1.5 $\times$6 mm orifice that separated the He source chamber from the scattering chamber. The longer axis of the rectangular He beam was perpendicular to the CO and laser beams. The back of the Jordan valve housing must be open to the air for cooling; we mounted the valve in a long housing that extended all the way through the source chamber and its rear flange. The valve was supported near the front by feedthroughs that permitted adjustments of the position along two axes perpendicular to the beam direction. The valve orifice was approximately 30 mm from the skimmer orifice and

130 mm from the intersection region. The valve was usually operated with 4–5 bar He. The pulse width, measured with a fast ionization gauge, was about 70 μs and the maximum He density at the crossing point was about 2×10^{13} atoms/cm^3.

Oil diffusion pumps evacuated both source chambers and the scattering chamber. The scattering chamber base pressure was about 2×10^{-7} Torr, and typical pressures during operation were ten times higher (mostly from He). The room-temperature background of CO was negligible during the experiments. The fragmentation pattern of the pump oil has no peak at mass 28, though ringing from the large peak at m/e 27 produced some noise.

The CO was probed by 2+1 REMPI through either the $B\,^1\Sigma^+$ or the $E\,^1\Pi$ states.[40,41] The second harmonic of an injection seeded Nd:YAG laser (Spectra-Physics/Larry Wolford Services) pumped a Continuum dye laser, and the dye laser output was doubled in a KDP crystal. The doubled output was then mixed with the YAG fundamental in KDP for probing through the B state near 230 nm, or with the dye laser fundamental in BBO for probing through the E state near 215 nm. The probe pulses were about 7 ns long and had energies on the order of 100 μJ. They were focused into the scattering volume by 250 mm or 100 mm lenses mounted inside the vacuum chamber. The probe laser beam propagated in the same plane as the two molecular beams and made an angle of 135° with the He beam. Its polarization was slightly elliptical with the major axis perpendicular to the beam plane. Most data came from the S branch of the $E\leftarrow X$ transition and the Q branch of the $B\leftarrow X$ transition.

DC electric fields accelerated the ions through a field-free flight tube 600 mm long and onto a 25 mm diameter microsphere plate detector (El-Mul). In Fig. 1, the ion flight path extends out of the page. The ion optics included a gridless extraction lens similar to that recently described by Eppink and Parker for velocity mapping experiments,[42] and a standard Einzel lens. The electron multiplier output current was preamplified and then collected by a Stanford Research Systems gated integrator for digitization. No analog averaging was used; the integrated signal at $m/e=28$ from each laser shot was digitized and all the data processing was performed afterwards. We usually collected eight samples with the He beam on and eight with it off at each wavelength.

During the experiments the He beam fired for two laser pulses and then remained off for two. We used the 2/2 alternation because the SRS integrator inserted a small error into its output that changed sign after each trigger, and therefore canceled if successive pairs of outputs were added together.

The timing of the experiment was controlled by a Real Time Devices programmable timer board and an SRS digital delay generator. A master 10 Hz clock with a fixed phase with respect to the ac power line reduced errors associated with 60 Hz interference.

III. RESULTS

Several measurements of the precollision CO rotational distribution all gave fractional populations in $j=0$ of $70\% \leqslant f_0 \leqslant 80\%$. Most of the remaining molecules had $j=1$, but the CO beam always contains a small population of higher j states that are not well cooled in the expansion; their rotational distribution corresponds to a temperature of approximately 250 K. For all final states $j\geqslant3$, the collision-induced change in the population was at least equal to, and often several times larger than, the initial population. The observed depletion of the $j=0$ state was about 5%.

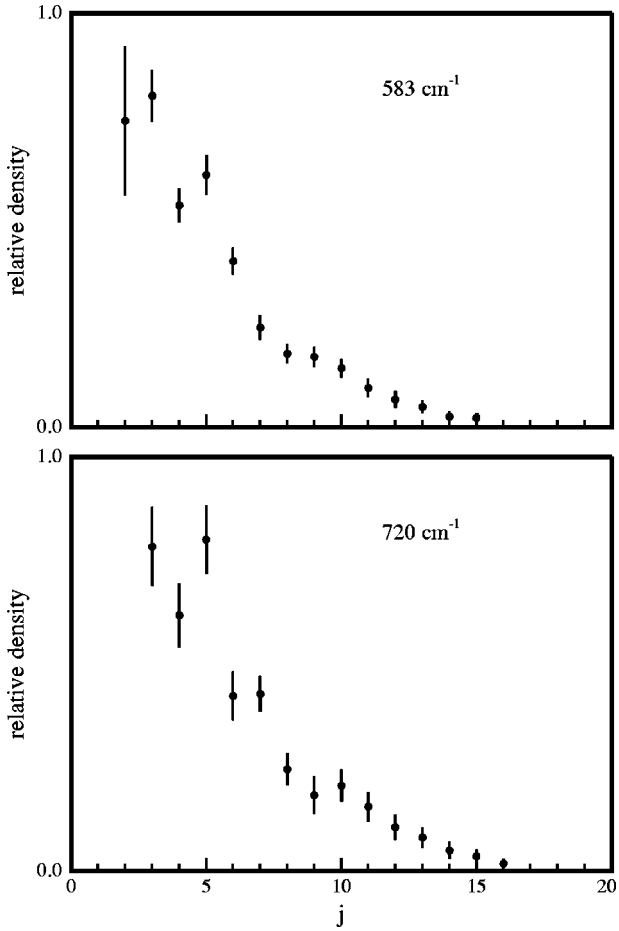

FIG. 2. Relative densities observed in the beam intersection region.

Figure 2 shows the relative densities of postcollision CO rotational states we observed. These densities were extracted from the observed signals via the expression

$$n(j)\propto\frac{(2j+1)(I_{\mathrm{on}}-I_{\mathrm{off}})}{S_j}. \tag{1}$$

I_{on} and I_{off} are the integrated line intensities observed with and without the He beam. Line strength factors S_j for the two-photon transitions were taken from Bray and Hochstrasser's paper.[43] Data points with $j<10$ were all obtained with the E intermediate state, and those with $j>14$ were all obtained with the B state. The two data sets were scaled to match at the intermediate levels and the points plotted there are averages of the two sets.

The error bars in Fig. 2 show $\pm2\sigma$ in the weighted means of several separate experimental runs; they represent both random error present in individual experiments and the reproducibility from one experiment to another, but do not include any estimates of possible systematic errors. The experiment provides only relative densities; the vertical scales in Fig. 2 are linear but arbitrary, and we did not attempt to compare intensities at the two different collision energies.

Systematic errors would occur if the relative intensities were dependent on the position of the laser beam waist within the scattering volume. We tested for such errors by deliberately placing the probe beam at four different positions in the intersection volume, but always within the cold central part of the CO beam, and collecting sample data sets. These experiments showed no systematic differences.

Another possible error was pointed out by Hines *et al.* in their paper on REMPI of CO through the E state.[41] Some ionized molecules appear in the C^+ mass channel rather than the CO^+ channel, and the branching ratio between the two depends on the probe pulse intensity, the spectroscopic branch and the rotational quantum number. The primary effect is systematic undercounting of high-j populations at high pulse energies. Hines *et al.* recommended that ions in both the C^+ and CO^+ channels should be collected and their spectra added before analysis. A background signal at mass 12 in our apparatus prevented us from taking that approach. Instead, we made several scans of thermal CO introduced into the chamber through a leak valve, with probe conditions identical to those used during the scattering experiment. Over the range of rotational states probed in our experiment, we found that straightforward analysis of the line intensities produced Boltzmann population distributions with accurate (299 K) temperatures. We concluded that under our conditions the branching ratio into the C^+ channel was either small or constant, and made no corrections for it in our data analysis.

If the scattered molecules have a net alignment in the laboratory, our measurements through the E state could be affected since we used only one laser polarization. Alexander and co-workers,[44–46] Mayne and Keil,[47] Follmeg *et al.*,[48] and Pullman *et al.*[49] have all published theoretical studies of alignment induced by rotationally inelastic collisions. The general conclusion of these studies is that the quadrupole alignment parameter $A_0^{(2)}$ is likely to be near zero for low Δj, but become negative as Δj increases. This conclusion is borne out in the experimental measurements of Meyer on He-NO collisions at 1185 cm^{-1}; he determined alignment parameters $A_0^{(2)}$ that decreased from zero at low Δj to approximately -0.4 at the highest Δj observed.[33] (A sample with $m_j=0$ for all molecules, where the projection is taken along the initial relative velocity, would have $A_0^{(2)}=-1$.)

We have used formulas given by Mo and Suzuki[50] and by Orr-Ewing and Zare[51] to evaluate the effect of such an alignment on our experimental distributions. For our geometry, the observed signal intensity is roughly

$$I(j)\propto n(j)[1+c(j)A_0^{(2)}], \tag{2}$$

where $c(j)$ increases slowly from about 0.24 at $j=3$ to 0.32 at $j=11$. We therefore expect that alignment effects cause a systematic *underestimation* of the densities as Δj increases, and that the error is on the order of 10% at the highest Δj we observe. We hope to determine these alignment parameters directly in a future experiment.

Measurements through the B state are unaffected by alignment, since we used the Q branch of this $\Delta\Lambda=0$ transition.[52]

IV. CALCULATIONS

A. Scattering calculations

We calculated integral and differential cross sections for He–CO scattering with the MOLSCAT program of Green and Hutson.[53] We used both the SAPT potential energy surface of Heijmen *et al.*[19] and the XC(fit) surface of Le Roy *et al.*[11] All the calculations treated CO as a rigid rotor; we used a version of the SAPT surface that was averaged over the ground state vibration of CO. Converged close-coupled (CC) calculations were performed at 583 cm^{-1} while at 720 cm^{-1} the coupled states (CS) approximation of McGuire and Kouri[54] was used. All calculations used the hybrid log-derivative/Airy propagator of Alexander and Manolopolous.[55]

MOLSCAT's built-in angular expansion routines were used; the potentials were expanded in a basis of thirteen Legendre functions, and 24-point Gauss-Legendre quadrature was used to evaluate the expansion coefficients. The rotational basis sets included all rotational channels $j\leqslant 18$ at 583 cm^{-1} and $j\leqslant 20$ at 720 cm^{-1}, so that all the open rotational channels and two closed channels were included. The sum over total angular momentum J terminated when the inelastic integral cross sections had converged to within 0.005 $Å^2$ and the elastic cross sections to within 1 $Å^2$. Convergence was tested with a series of CS calculations at 583 cm^{-1}. The results were insensitive to reasonable changes in propagator step size, the changeover point between the short-range and long-range propagators, the number of Legendre functions and quadrature points in the potential expansion, the maximum distance for the propagation, the upper limit of J in the partial wave sum, and the total number of rotational states included in the basis.

We performed both CS and CC calculations at 583 cm^{-1}. At that energy, the CS calculations took about seven minutes while the CC calculations took about two days on a modest desktop computer. The differences between the CS and CC integral cross sections σ_{if} for the $j=i\rightarrow j=f$ rotational transitions were smaller than our experimental uncertainties in all cases. The agreement was better at higher Δj; the largest difference between CC and CS results for σ_{0j} was 0.13 $Å^2$ at $j=3$, and for $j\geqslant 6$ the differences were all less than 0.07 $Å^2$. Differential cross sections from CS calculations tended to have their rotational rainbow maxima shifted a few degrees toward higher scattering angle from the CC results, and the phases of the rapid oscillations at low angles were quite different for some transitions. Nonetheless, the shapes and amplitudes of the CS differential cross sections usually agreed well with the CC ones.

The CS approximation is an impulsive approximation and should become more accurate as the collision energy increases. We concluded that the CS calculations were sufficiently accurate for comparison with our integral cross section data at the higher 720 cm^{-1} collision energy, and did not perform CC calculations there. The accuracy of the CS calculations is not surprising; the He–CO attractive well is only about 25 cm^{-1} deep, so collisions at energies above 500 cm^{-1} should be largely impulsive.

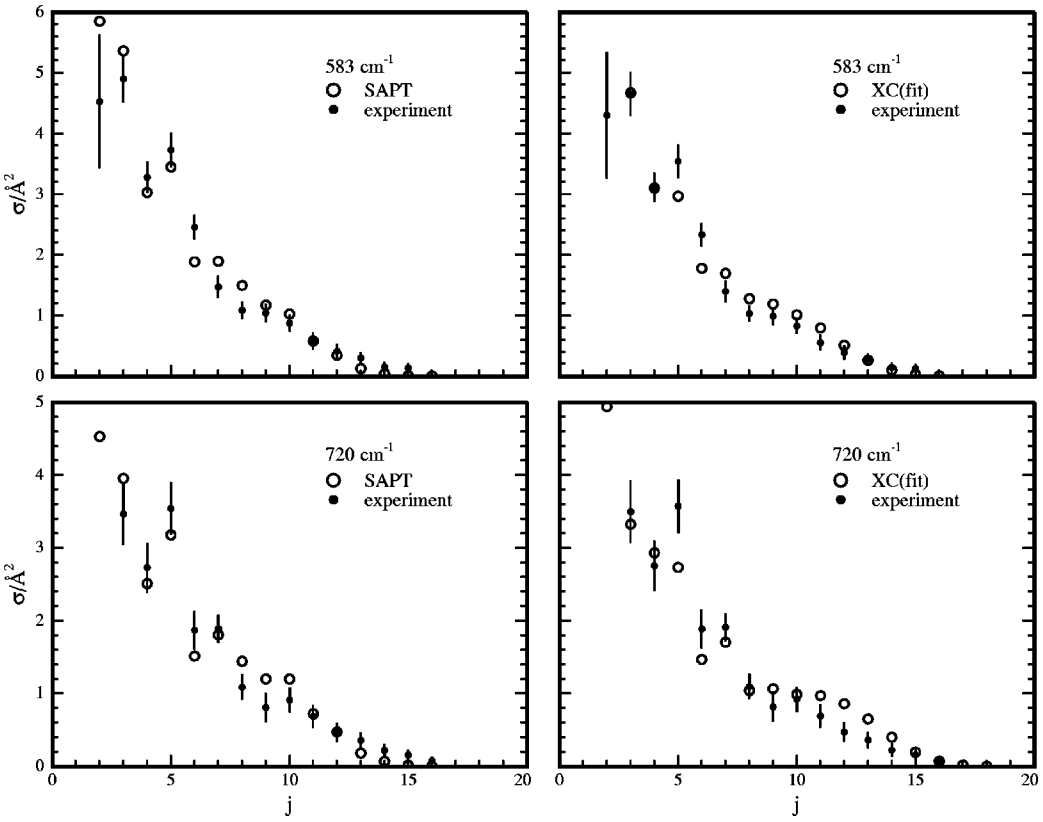

FIG. 3. Calculated cross sections compared to data. Open circles show theoretical cross sections, weighted for the initial populations of rotational levels in the beam and the density-to-flux transformation. Filled circles show experimental data, scaled to match the total inelastic cross section into $j \geqslant 3$.

B. Density to flux corrections

The REMPI signal measures the density of molecules in the focal volume of the probe laser. The density is not necessarily proportional to the cross section for production of the detected state, since molecules in some final states will tend to leave the detection volume more rapidly than others. Several authors have discussed the necessary ''density-to-flux'' transformation.[56–59] It is necessary to know the state-to-state *differential* cross sections in order to evaluate the *j*-specific relative sensitivities needed for extraction of state-to-state *integral* cross sections from experimental data.

Naulin *et al.* published the most general approach to the density-to-flux transformation yet available.[57] Their calculation accounts realistically for the shape of the molecular beam intersection region and the time dependence of the pulsed beams. In our experiment, the CO molecules are scattered into a fairly small solid angle by the light He, the probe volume is small compared to the molecular beam intersection volume, and the molecular beam durations are long compared to the flight time through the detection volume. Therefore the simpler approach of Dagdigian[59] is appropriate:

$$\sigma_{if} = \frac{n_f}{n_i n_t R \left\langle \frac{g}{v_f} \right\rangle_{if}}. \tag{3}$$

In Eq. (3), σ_{if} is the integral cross section for the $i \rightarrow f$ transition, n_f is the measured final-state density, n_i and n_t are the initial densitities of the target (CO) and projectile (He) beams, R is the effective radius of the intersection region, g is the initial relative velocity, and v_f is the final laboratory frame speed of a scattered molecule. The average is performed over all scattering angles, weighted by the differential cross section:

$$\left\langle \frac{g}{v_f} \right\rangle_{if} = \int \left(\frac{g}{v_f} \right) \sigma_{if}^{-1} \left(\frac{d\sigma}{d\omega} \right)_{if} d\omega, \tag{4}$$

where $\sigma_{if}^{-1}(d\sigma/d\omega)_{if}$ is the normalized differential cross section for the $i \rightarrow f$ transition.

We used Eq. (4) to determine the density-to-flux correction factors $\langle g/v_f \rangle_{if}$ for our experiment. To provide the fairest comparison between calculated and experimental cross sections, we calculated the correction factors separately from each potential surface and applied them to the calculated cross sections as described below.

C. Results

The open symbols in Fig. 3 give the inelastic cross sections from scattering calculations on the XC(fit) and SAPT potential surfaces. The symbols show the weighted cross sections

$$\sigma(j) = \sigma_{0j} f_0 \left\langle \frac{g}{v_f} \right\rangle_{0j} + \sigma_{1j} f_1 \left\langle \frac{g}{v_f} \right\rangle_{1j}, \tag{5}$$

where σ_{0j} and σ_{1j} are the calculated integral cross sections and f_0 and f_1 are the fractional populations in the two lowest rotational states in the CO beam. f_0 was taken as 70% in the 583 cm^{-1} experiment and 76% in the 720 cm^{-1} experiment, corresponding to the averages of measurements made during those experimental runs. The experimental data from Fig. 2 also appear in each panel, scaled so that the sum of all the $\sigma_{exp}(j)$ for $j \geqslant 3$ matched the corresponding sum from the calculation. (The experimental point at $j=2$ is the result of a single measurement and had the largest background correction; we did not use it in the scaling procedure.) The effects of the density-to-flux corrections are small; He is so light compared to CO that even strongly backscattered CO molecules do not deviate very much from their initial velocities, so the density-to-flux factors $\langle g/v_f \rangle_{if}$ are all very similar. We normalized the factors so that the vertical axis in Fig. 3 can still be interpreted as an absolute cross section.

V. DISCUSSION

Oscillatory structure is present in the low-j experimental rotational distributions at both collision energies. As discussed in the Introduction, this structure arises from competition between terms with even and odd orders in the Legendre expansion of the potential. Our experimental data display a clear preference for odd j below $j \approx 8$, and a less convincing bump at $j=10$ in the 720 cm^{-1} distribution.

The XC(fit) potential gives cross sections that show a monotonic, though stepped, decrease with j at 583 cm^{-1}. At 720 cm^{-1} the fall is again steady except for $j=7$. The SAPT potential, on the other hand, does capture the low-j oscillations reasonably well. Both potentials predict nearly equal populations in $j=6$ and 7 at 583 cm^{-1}, and a slight rise from 6 to 7 at 720 cm^{-1}; the experiment shows a relatively steep drop at the lower energy and nearly equal populations at the higher one. The XC(fit) potential slightly overestimates the importance of transitions with $\Delta j \geqslant 10$, especially at 720 cm^{-1}.

Figure 4 shows the calculated cross sections for excitation out of $j=0$ and 1 separately for the two potential surfaces at the collision energy 583 cm^{-1}. Oscillatory structure is present for both initial states in both figures, but is more pronounced in the SAPT result. The differences between the two results must be due to differences in the potential surfaces, since the scattering calculations at this energy were essentially exact.

The experiment measures a weighted sum of the cross sections out of $j=0$ and 1, where the weighting factors are the fractional populations of the two initial states in the CO beam. In the limit of a perfectly cold beam, the experimental result would correspond to the $\sigma_{0\to j}$ trace; if the initial populations f_0 and f_1 were equal, it would correspond to a simple average of the two. Results ranging from strong oscillations to a monotonic decrease could be expected for initial population distributions between those two extremes. The SAPT surface shows much deeper interference oscillations in the unweighted cross sections than the XC(fit) surface, and those oscillations are not entirely damped by the average over initial rotational populations in our beam. The weaker oscillations in the XC(fit) results do not survive the averaging over initial populations. We conclude that the SAPT potential gives a better account of the anisotropy of the He–CO interaction at the energies of our experiment.

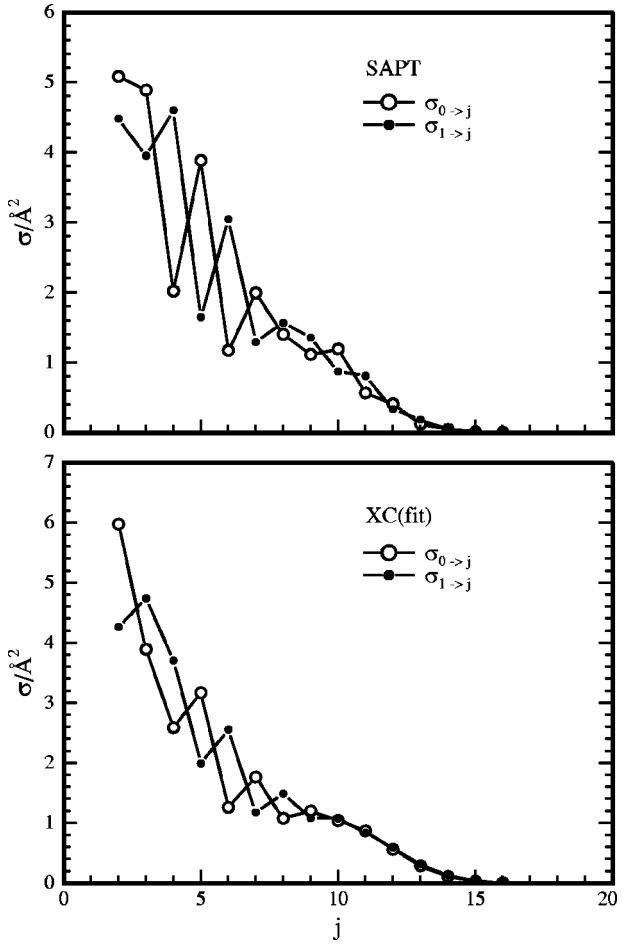

FIG. 4. Cross sections out of $j=0$ and 1 for the two surfaces at 583 cm^{-1}.

Figure 5 shows the 200 cm^{-1} and 583 cm^{-1} contours for both potential surfaces. The contours at 720 cm^{-1} have similar shapes but are shifted another 0.08 bohr to lower distances. The contours shown in Fig. 5 are therefore repre-

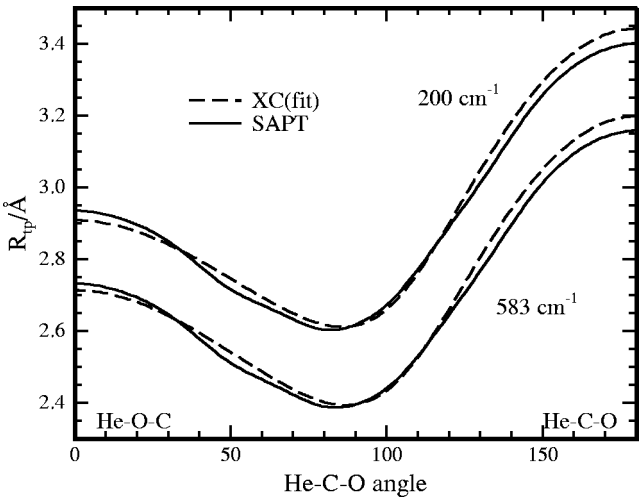

FIG. 5. Energy contours in the repulsive region for both surfaces.

sentative of the differences in the two surfaces over most of the repulsive region relevant to our experiment.

The two surfaces are very similar. The difference between the two ends of the molecule is larger in the XC(fit) potential, but the SAPT potential is steeper (has a stronger local anisotropy) in the region around 35°. It is difficult to make precise statements about the relation between the contours in the repulsive region and the calculated integral cross sections shown in Fig. 4. Nonetheless we speculate that the larger difference between the C and O ends of the molecule in the XC(fit) potential contributes a larger ''odd anisotropy'' and induces stronger damping in the even-odd oscillations as discussed by McCurdy and Miller.[26]

VI. CONCLUSIONS

Measured state-to-state rotational energy transfer cross sections have been compared with scattering calculations on two high-quality potential surfaces. The data are sensitive to the repulsive wall of the He–CO interaction. The XC(fit) surface, which is known to be very accurate in the van der Waals region and also reproduces several different transport properties accurately, does not reproduce the inelastic cross sections as well as the *ab initio* SAPT surface.

ACKNOWLEDGMENTS

The authors thank A. van der Avoird and R. J. Le Roy for potential surface codes and for useful comments and suggestions, and F. C. DeLucia and C. Ball for initial help with the calculations. Acknowledgement is made to the Donors of The Petroleum Research Fund, administered by the American Chemical Society, for support of this research. Additional support from the Department of Chemistry at Ohio State University and the Ohio Supercomputer Center is gratefully acknowledged.

[1] M. Thachuk, C. E. Chuaqui, and R. J. Le Roy, J. Chem. Phys. **105**, 4005 (1996).
[2] H. P. Butz, R. Feltgen, H. Pauly, and H. Vehmeyer, Z. Phys. **247**, 70 (1971).
[3] R. B. Nerf, Jr. and M. A. Sonnenberg, J. Mol. Spectrosc. **58**, 474 (1975).
[4] M. Keil, J. T. Slankas, and A. Kuppermann, J. Chem. Phys. **70**, 541 (1979).
[5] M. Faubel, K. H. Kohl, and J. P. Toennies, J. Chem. Phys. **73**, 2506 (1980).
[6] D. Bassi, A. Boschetti, S. Marchetti, G. Scoles, and M. Zen, J. Chem. Phys. **74**, 2221 (1981).
[7] L. D. Thomas, W. P. Kraemer, and G. H. F. Diercksen, Chem. Phys. **51**, 131 (1980).
[8] W. Dilling, Ph.D. thesis, University of Göttingen, Germany, 1985, cited in Ref. 9.
[9] F. A. Gianturco, N. Sanna, and S. Serna-Molinera, Mol. Phys. **81**, 421 (1994).
[10] C. E. Chuaqui, R. J. Le Roy, and A. R. W. McKellar, J. Chem. Phys. **101**, 39 (1994).
[11] R. J. Le Roy, C. Bissonnette, T. H. Wu, A. K. Dham, and W. J. Meath, Faraday Discuss. **97**, 81 (1994).
[12] R. Moszynski, T. Korona, P. E. S. Wormer, and A. van der Avoird, J. Chem. Phys. **103**, 321 (1995).
[13] F.-M. Tao, S. Drucker, R. C. Cohen, and W. Klemperer, J. Chem. Phys. **101**, 8680 (1994).
[14] B. Kukawska-Tarnawska, G. Chałasiński, and K. Olszewski, J. Chem. Phys. **101**, 4964 (1994).
[15] A. Dham and W. Meath, Mol. Phys. **88**, 339 (1996).
[16] F. A. Gianturco, F. Paesani, M. F. Laranjeira, V. Vassilenko, M. A. Cunha, A. G. Shashkov, and A. F. Zolotoukhina, Mol. Phys. **92**, 957 (1997).
[17] M.-C. Chan and A. R. W. McKellar, J. Chem. Phys. **105**, 7910 (1996).
[18] E. Heck and A. Dickinson, Mol. Phys. **91**, 31 (1997).
[19] T. G. A. Heijmen, R. Moszynski, P. E. S. Wormer, and A. van der Avoird, J. Chem. Phys. **107**, 9921 (1997).
[20] J. P. Reid, P. W. Barnes, and C. J. S. M. Simpson, Chem. Phys. Lett. **280**, 359 (1997).
[21] F. A. Gianturco, F. Paesani, M. F. Laranjeira, V. Vassilenko, M. A. Cunha, A. G. Shashkov, and A. F. Zolotoukhina, Mol. Phys. **94**, 605 (1998).
[22] E. J. Kruus, J. Phys. Chem. **98**, 3099 (1994).
[23] P. Brumer, Chem. Phys. Lett. **28**, 345 (1974).
[24] S. Green and P. Thaddeus, Astrophys. J. **205**, 766 (1976).
[25] S. D. Augustin and W. H. Miller, Chem. Phys. Lett. **28**, 149 (1974).
[26] C. W. McCurdy and W. H. Miller, J. Chem. Phys. **67**, 463 (1977).
[27] M. M. Maricq, J. Chem. Phys. **103**, 5999 (1995).
[28] T. Orlikowski and M. H. Alexander, J. Chem. Phys. **79**, 6006 (1983).
[29] M. H. Alexander, J. Chem. Phys. **99**, 7725 (1993).
[30] P. Andresen, H. Joswig, H. Pauly, and R. Schinke, J. Chem. Phys. **77**, 2204 (1982).
[31] H. Joswig, P. Andresen, and R. Schinke, J. Chem. Phys. **85**, 1904 (1986).
[32] A. V. Smith and A. W. Johnson, Chem. Phys. Lett. **93**, 608 (1982).
[33] H. Meyer, J. Chem. Phys. **102**, 3151 (1995).
[34] R. Fei, H. M. Lambert, T. Carrington, S. V. Filseth, C. M. Sadowski, and C. H. Dugan, J. Chem. Phys. **100**, 1190 (1994).
[35] N. Furio, A. Ali, and P. J. Dagdigian, J. Chem. Phys. **85**, 3860 (1986).
[36] G. Jihua, A. Ali, and P. J. Dagdigian, J. Chem. Phys. **85**, 7098 (1986).
[37] P. J. Dagdigian, D. Patel-Misra, A. Berning, H.-J. Werner, and M. H. Alexander, J. Chem. Phys. **98**, 8580 (1993).
[38] R. G. Macdonald and K. Liu, J. Chem. Phys. **97**, 978 (1992).
[39] D. Proch and T. Trickl, Rev. Sci. Instrum. **60**, 713 (1989).
[40] G. W. Loge, J. J. Tiee, and F. B. Wampler, J. Chem. Phys. **79**, 196 (1983).
[41] M. A. Hines, H. A. Michelsen, and R. N. Zare, J. Chem. Phys. **93**, 8557 (1990).
[42] A. T. J. B. Eppink and D. H. Parker, Rev. Sci. Instrum. **68**, 3477 (1997).
[43] R. G. Bray and R. M. Hochstrasser, Mol. Phys. **31**, 1199 (1976).
[44] M. H. Alexander and P. J. Dagdigian, J. Chem. Phys. **66**, 4126 (1977).
[45] M. H. Alexander, J. Chem. Phys. **67**, 2703 (1977).
[46] T. Orlikowski and M. H. Alexander, J. Chem. Phys. **80**, 4133 (1984).
[47] H. R. Mayne and M. Keil, J. Phys. Chem. **88**, 883 (1984).
[48] B. Follmeg, P. Rosmus, and H.-J. Werner, J. Chem. Phys. **93**, 4687 (1990).
[49] D. Pullman, B. Friedrich, and D. Herschbach, J. Phys. Chem. **99**, 7407 (1995).
[50] Y. Mo and T. Suzuki, J. Chem. Phys. **109**, 4691 (1998).
[51] A. J. Orr-Ewing and R. N. Zare, Annu. Rev. Phys. Chem. **45**, 315 (1994).
[52] R. J. Gordon and G. E. Hall, Adv. Chem. Phys. **XCVI**, 1 (1996).
[53] J. M. Hutson and S. Green, MOLSCAT computer code, version 14 (1994), distributed by Collaborative Computational Project No. 6 of the Engineering and Physical Sciences Research Council (UK).
[54] P. McGuire and D. J. Kouri, J. Chem. Phys. **60**, 2488 (1974).
[55] M. H. Alexander and D. E. Manolopoulos, J. Chem. Phys. **86**, 2044 (1987).
[56] H. W. Cruse, P. J. Dagdigian, and R. N. Zare, Faraday Discuss. Chem. Soc. **55**, 277 (1973).
[57] C. Naulin, M. Costes, A. Benseddik, and G. Dorthe, Laser Chem. **8**, 283 (1988).
[58] D. M. Sonnenfroh and K. Liu, Chem. Phys. Lett. **176**, 183 (1991).
[59] P. J. Dagdigian, in *Atomic and Molecular Beam Methods, Vol. I*, edited by G. Scoles (Oxford University Press, New York, 1988).